Statistical Assessment of the Variability of Atmospheric Propagation Effects in the Southern California Coastal Area

L. Ted Rogers
Naval Command Control and Ocean Surveillance Center
NCCOSC RDTE DIV 543
53170 WOODWARD ROAD
SAN DIEGO CA 92152-7385 USA
T: 619.553.1413 F: 619.553.1417 Email: trogers@nosc.mil

The effect from horizontal inhomogeneity in the atmospheric refractive structure on radio frequency (RF) propagation is a current subject of discussion. Meteorological measurements indicating range dependent refractive structures have been documented by several observers (Goldhirsh and Dockery, 1991, Anderson, 1991, Levy and Craig, 1991.) A central concern arising from these observations is the effect the assumption of horizontal homogeneity has on the accuracy of propagation estimates, where accuracy is defined as the difference between estimated and actual propagation effects, typically pathloss. Whether the environment can be considered homogeneous is dependent upon the accuracy requirements of the application and the accuracy of pathloss estimates developed from environmental inputs, i.e. what is the accuracy obtained assuming horizontal homogeneity, how much does that accuracy improve with the inclusion of range dependent refractive structures, and what is the reduction in accuracy of either regime as a function of the time since the observation used for developing estimates.

The Variability Of Coastal Atmospheric Refractivity (VOCAR) experiment was designed to assess the effects of spatial and temporal variability of the atmospheric refractive structure in the southern California coastal (SoCal) area on RF pathloss. Three months of RF pathloss measurements on two ~ 130 km over-water, over-the-horizon paths having a common endpoint but on radials separated by 120 degrees are used to assess the effects of spatial and temporal inhomogeneity on RF pathloss. Mid-path atmospheric soundings from a four day period are compared to measured pathloss values to examine the errors arising from the assumption of horizontal homogeneity. The increase in error when the path is moved away from the point of the sounding is also analyzed and compared.

EXPERIMENTAL SETUP

Figure 1. illustrates the geographical layout of the VOCAR experiment. Three CW transmitting systems at 143.09, 262.85, and 374.95 MHz are installed at the northwest end of San Clemente Island (33-01.4 N, 118-35.2 W). Receiving systems are located at Naval Air Warfare Center Weapons Division (NAWCWPNS), Point Mugu (34-07.2 N, 119-07.2 W) and Naval Command Control and Ocean Surveillance Center RDT&E Division, San Diego (32-41.8 N, 117-15.18 W). Path "A" in Figure 1 is from the transmitting site on San Clemente Island to the receiving site at Point Mugu. Path "B" in Figure 1 is from the same transmit site to the receiving site in San Diego.

The CW links provide detectable signal levels at the receiver sites under standard atmosphere conditions. Each transmitting system consists of a transmitter, cables, a power divider, and two Yagi-Uda antennas, one aligned with the azimuth for path A and the other aligned with the azimuth for path B. Each receiving system consists of a log periodic antenna, a spectrum analyzer used as a receiver and also a personal computer used for control and data recording. Path geometry parameters are listed in the first four rows of Table 1. The next three rows of Table 1 are the standard atmosphere propagation factors (pathloss referenced to free space pathloss) computed using the geometry parameters and frequency as input to the EREPS program (Patterson, et al., 1990.)

TABLE 1. *Geometry and standard atmosphere propagation factors for VOCAR CW links.*

Path	A	B
Transmitter height (m)	18.4	16.6
Receiver height (m)	30.5	30.5
Path length (km)	132.6	127.2
Azimuth to receiver (deg.)	337	106
Standard propagation factor at 143.09 MHz	50.4	50.4
Standard propagation factor at 262.85 MHz	49.1	49.0
Standard propagation factor at 374.95 MHz	49.4	49.4

Receiving systems were operated in 15 minute cycles. Within each 15 minute cycle, five sampling cycles were run. During each sampling cycle, at each of 17 frequencies, (including the 3 CW frequencies this report is concerned with) instantaneous measurements of peak amplitude, peak amplitude frequency and noise level were measured and stored. After the fifth sampling cycle, the measurements were averaged and recorded to disk. The data were smoothed using a 2-hour wide triangular window.

LONG TERM OBSERVATIONS

The purpose of long term observations is to characterize the effects of the spatial and temporal variability of refractivity on the received signal levels on paths A and B. Figure 2. is a time series of the received signal level (RSL) at 262.85 MHz on both path A and path B for the period June 1, 1993 through September 7, 1993. The abscissa is days of the year and the ordinate is the RSL in dBm The most striking feature is the large portion of time that signals are above troposcatter levels. It is observed that the gross features are largely homogeneous, that is, when there are elevated signal levels on path A there are also elevated signal levels on path B. Short term deviations from the mean value over fractions of a day do not appear to be correlated between the two paths. Plot of the signals at 143.09 MHz and 374.95 MHz (not included in this paper) are similar in appearance.

Correlation

The linear autocorrelations and the cross correlation for the 262.85 MHz signals on both paths A and B are plotted in Figure 3. The abscissa is from -384 to 384 lag hours, i. e. hours that the signal on path B lag the signals on path A. The solid line is the autocorrelation of the path A signal and the dotted line is the autocorrelation of the path B signal. Differences between the two are very slight. The long dashed line is the cross correlation between the path A and path B signals. Using this abscissa scale the cross correlation appears very close to the autocorrelation except in the immediate vicinity of zero lags, where it reaches a maximum value of 0.78.

A reduced abscissa scale is used in Figure 4 to provide better detail of the 262.85 MHz correlation and autocorrelation functions in the vicinity of zero lags. The peak cross correlation occurs at approximately 1.5 hours of lag and the cross correlation function is nearly symmetric about its peak. This could be explained as a large component of the signal level amplitude on path B being a time shifted function of the signal amplitude on path A. The time shifted component will be the convolution of the autocorrelation with the probability density function of the shift. If the time shift density function is symmetric about some mean, the cross correlation will also be symmetric about that mean.

Error with an ideal estimator

The concept of an ideal estimator is useful for examining the degradation of accuracy in pathloss estimates as a function of the time difference between the time of an observation used to make those estimates and the time of the use of the estimates. If $y(t)$ is an ideal estimator of $x(s)$ then $y(t)$ is equal to $x(s)$ when t is equal to s and the cross correlation function of $x(t)$ and $y(s)$ is equal to the autocorrelation function of $x(t)$ and $x(s)$. The standard deviation of the error, or *standard error* of $y(t)$ in estimating $x(s)$ is calculated directly or from correlation functions of $x(s)$ and $y(t)$ and their standard deviations. In Figures 5, 6 and 7, the standard error of the ideal estimator of the current RSL on path A ("path A" in the legend) is plotted as a function of the time lag (or delay) since the ideal estimator was current. When the estimate is current (Lag hours equal to zero) there is no error, however there is a very rapid increase in error in the first four hours with the error curve flattening out after that point. In the same graphs appear the estimation errors obtained using the RSL on path B to estimate the RSL on path A as a function of the time since the RSL on path B was observed. "Leading" and "lagging" plots are provided as the cross correlation functions between path A and path B are not symmetric.

The important point that is illustrated in Figures 5, 6 and 7 is that there is a calculable trade-off in estimation accuracy between the effects of spatial and temporal variability. Using the 262.85 MHz signal as an example, real time pathloss (zero lag) information from path B is as accurate as ideal pathloss information from path A that is eight hours old. At 16 hours of lag, the information from path A is no better than the information from path B in predicting the pathloss on path A.

COMPARISONS WITH RADIOSONDE BASED PATHLOSS ESTIMATES

From August 25, 1993 to August 30, 1993, the Research Vessel Point Sur remained within 10 km of the mid-point of the path from San Clemente Island to Point Mugu (path A). During that period, twenty seven radiosondes were launched from the ship at four hour intervals. The modified refractivity profiles (M-profiles) calculated from the soundings and the path geometry's given in Table 1 have been used as inputs to the Radio Physical Optics program (Hitney, 1992) to calculate pathloss values for both path A and path B. A time series of the described M-profiles appears in Figure 8. Measurements of the accuracy of the pathloss estimates for path A are examined and compared to the measurements of the accuracy of the estimates for path B.

Time series

The measured and calculated propagation factor at 262.85 MHz for both path A and path B are plotted in Figure 9. The abscissa is aligned with that of the preceding plot of the M-profiles from the R. V. Point Sur radiosondes. The ordinate is the propagation factor in dB. It is seen that the measured signal on both paths remains within 10 to 20 dB of free space until day 240 when the average signal level drops to about -30 dB. The transition in propagation factors corresponds in time to the transition from surface based to an elevated duct seen in the previous plot. The calculated estimates of the propagation factor for path A follow the measured values reasonably well and appear to be unbiased. A notable feature is a ripple with a mean period of approximately 4 hours in the measured values. These short term fluctuations are present throughout the VOCAR data and are reflected in the steep slope of the autocorrelation functions in the vicinity of zero lags

Statistics

Table 2 provides the accuracy of the calculated pathloss estimates discussed in the preceding paragraphs. The first column of Table 2 lists the frequency. For the second column, an "A" is the comparison for measured and calculated propagation factor on path A, a "B" is the same for path B, and "B-A" is the difference between the statistics for path A and path B. Columns three through six are the statistics of the accuracy of the propagation factor estimates, RMS error, standard error, bias and correlation (Corr.) Table 3 lists the RMS error associated with the assumption of free space and then standard atmosphere environments and Table 4 lists the errors for using the propagation factor on path B to estimate the propagation factor on path A.

TABLE 2. *Error statistics of sounding based propagation factor estimates.*

Frequency (MHz)	Path	RMS error (dB)	Std. Error (dB)	Bias (dB)	Corr.
143.09	A	5.68	5.44	-0.85	0.75
143.09	B	10.07	7.87	-6.27	0.70
143.09	A-B	4.57	2.44		
262.85	A	7.30	7.30	0.0	0.76
262.85	B	8.52	8.26	-2.09	0.69
262.85	A-B	1.22	0.96		
374.95	A	7.36	7.23	1.34	0.79
374.95	B	9.61	9.27	-2.51	0.70
374.95	A-B	2.52	2.04		

TABLE 3. *Free space and standard atmosphere RMS error in estimating pathloss on path A.*

Frequency (Mhz)	Free Space (dB)	Standard Atmosphere (dB)
143.09	24.11	27.33
262.85	16.20	37.06
374.95	13.46	41.61

TABLE 4. *Error statistics for using propagation factor on path B to predict the propagation factor on path A.*

Frequency (Mhz)	RMS Error (dB)	Standar d Error (dB)	Bias (dB)	Corr. (dB)
143.09	8.30	5.97	5.76	0.75
262.85	7.21	6.68	2.72	0.76
374.95	7.96	7.05	3.68	0.79

At all three frequencies, the RMS error using calculations based upon the described soundings as estimators of the measured propagation factor is less than one half the RMS error obtained using the free space propagation factor as the estimator and less than one quarter the RMS error obtained using the standard atmosphere propagation factor as the estimator. It is seen that the accuracy of estimating the propagation factor on path A using the propagation

factor at the same frequency from path B is of roughly the same accuracy as using the estimates based upon the mid-path soundings. It should also be noted that the bias terms (the mean of the measured values minus the mean of the estimates) obtained for estimating the propagation factor on path A using the mid-path soundings are all less than 2 dB in magnitude indicating good performance on the part of the model.

CONCLUSIONS

What constitutes sufficient horizontal homogeneity for the assumption of horizontal homogeneity to be considered valid is dependent upon the application. Using the VOCAR experiment as a reference point the arguments for homogeneity might be as follows: If 4 dB RMS error is required for estimates of the pathloss on path A, neither mid-path radiosondes nor measured loss values from path B would provide sufficient accuracy, therefore an assumption of horizontal homogeneity would be invalid. Conversely, if the required RMS error is 10 dB then the refractive environment is sufficiently homogeneous to estimate the loss on path B using the sounding taken on path A, as well as by using the loss on path A, so the assumption of horizontal homogeneity would be valid.

While it is not strictly correct to compare findings from the short period of time when R. V. Point Sur soundings were taken with those from the long term measurements, there are noteworthy observations to be made. At 262.85 MHz the standard error for estimating the propagation factor on path A using mid-path soundings was found to be 7.30 dB. In Figure 6, the time delayed loss value on path A is at that error level at plus and minus 6 hours of lag (it is symmetric) and both the path B leading and lagging estimators (the respective losses on path B) are at that error level at plus and minus two hours of lag. This illustrates the trade-off between spatial and temporal variability that must be considered when comparing propagation prediction systems.

REFERENCES

Goldhirsh, J. and G.D. Dockery, "Propagation measurements and modeling at C band for over-the-water, line-of-sight propagation links in the Mid-Atlantic coast," Radio Science, Volume 26, No. 2, pp. 671-690, May-June 1991

Anderson, K.D. "Remote Sensing of the Evaporation Duct Using an X-Band Radar," AGARD Conference Proceeding 502, pp. 3.1 - 3.9, 1991

Levy, M.F. and K.H. Craig, "Use of Mesoscale Models for Refractivity Forecasting," ," AGARD Conference Proceeding 502, pp. 7.1 - 7.12, 1991

Patterson, W. L. , et al., "Engineers Refractive Effects Prediction System (EREPS) 2.0" NOSC Tech. Doc. 1342, Revision 2.0, 1990

Hitney, H.V. "Hybrid Ray Optics and Parabolic Equation Methods For Radar Propagation Modeling," IEE Radar 92 Conference Proceedings No. 365, pp. 58 - 61, 1992

FIGURE 1. Layout of VOCAR CW links.

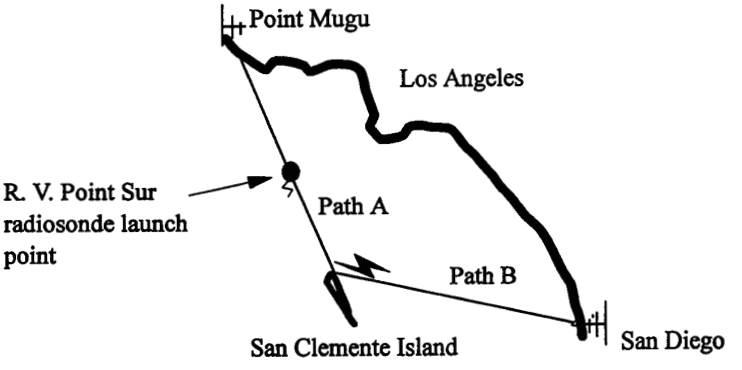

FIGURE 2. Time series of 262.85 MHz propagation factors for path A and path B.

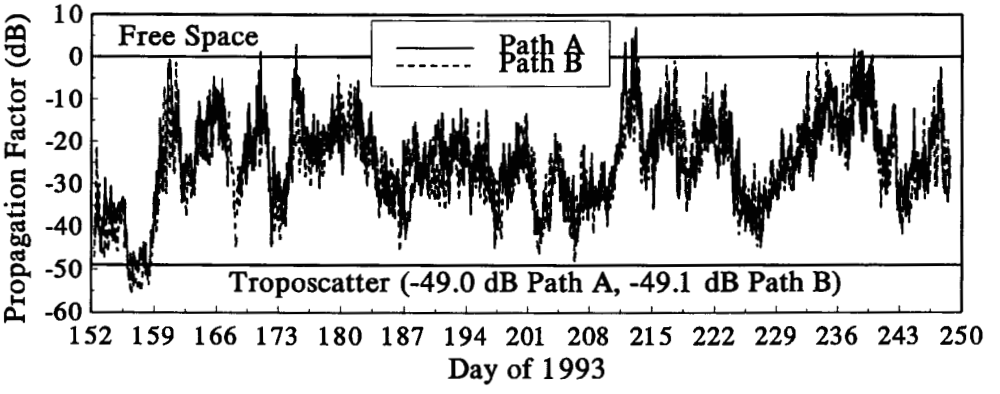

FIGURE 3. Correlation at 262.85 MHz (full abscissa.)

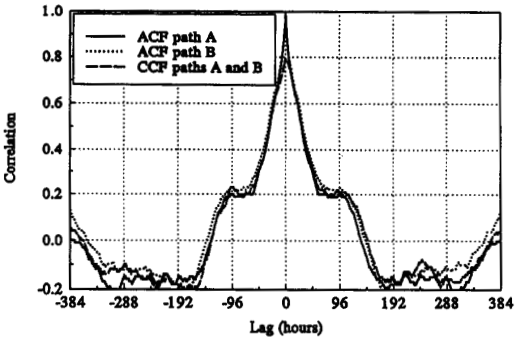

FIGURE 4. Correlation at 262.85 MHz (reduced abscissa.)

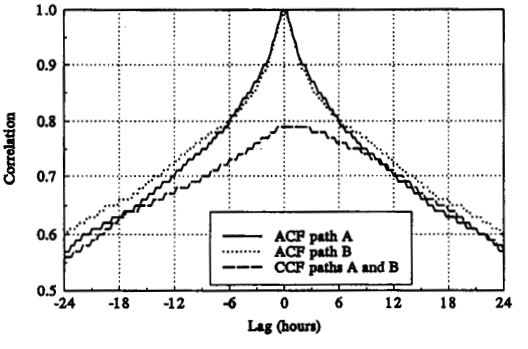

FIGURE 5. Delay error at 143.09 MHz

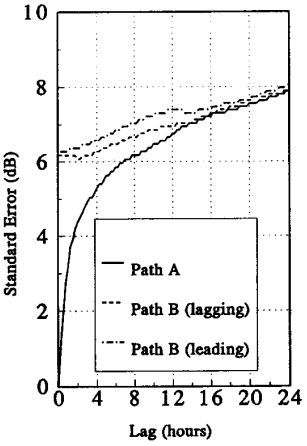

FIGURE 6. Delay error at 262.85 MHz

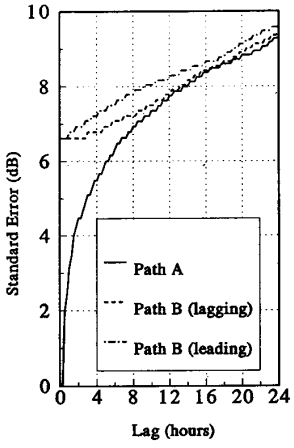

FIGURE 7. Delay error at 374.95 MHz

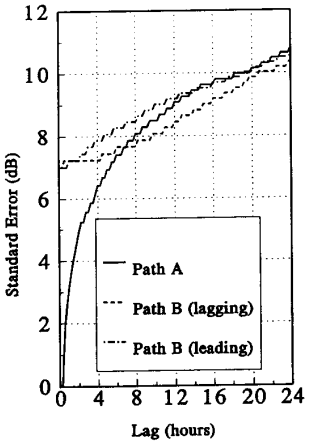

FIGURE 8. Time series of M-profiles from R. V. Point Sur atmospheric soundings.

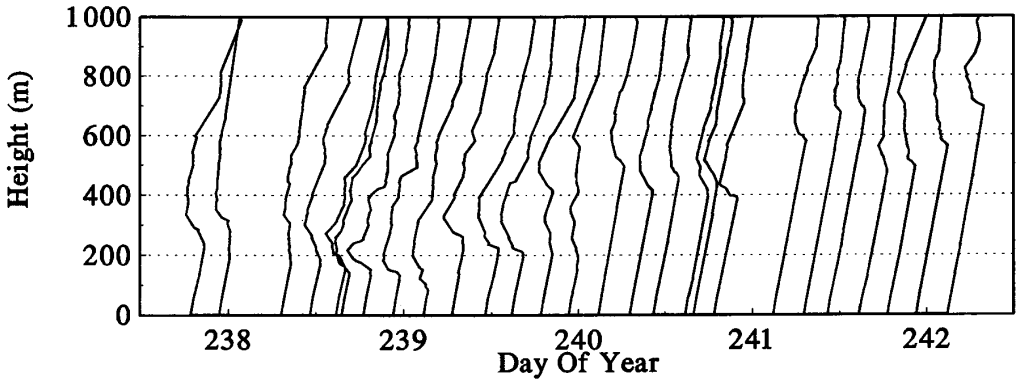

FIGURE 9. Time series of measured and calculated propagation factor at 262.85 MHz for path A and path B.